# Treatment Planning for a Radiosurgical System with General Kinematics

Achim Schweikard [⋆†] Rhea Tombropoulos [⋆‡] Lydia Kavraki [⋆]
John R. Adler [†] Jean-Claude Latombe [⋆]
[⋆] Robotics Laboratory, Department of Computer Science
[†] Department of Neurosurgery
[‡] Section on Medical Informatics, School of Medicine
Stanford University, Stanford, CA 94305, USA, as@cs.stanford.edu

**Abstract:** *In radiosurgery a beam of radiation is used as an ablative surgical instrument to destroy brain tumors. Treatment planning consists of computing a sequence of beam configurations for delivering a necrotic dose to the tumor, without damaging healthy tissue or particularly critical structures. In current systems, kinematic limitations severely constrain beam motion. This often results in inappropriate dose distributions. A new radiosurgical system has been implemented to overcome this disadvantage. In this system, a compact radiation source of high energy is moved by a 6-dof robotic arm. We describe algorithms for computing a motion with specified characteristics for this new system. Treatment plans used at test sites with earlier systems are compared to plans computed with the described algorithms. The experience reported shows that full kinematic flexibility combined with treatment planning algorithms allows for better protection of healthy tissue and higher dosage in tumors.*

**Acknowledgments:** This research is funded in part by the Sheik Enany Fund, Lorraine Ulshafer Fund and by the National Library of Medicine (LM-05305 and LM-07033). The authors thank Mohan Bodduluri, Joe Depp, and Bo Preising of Accuray Inc. for their help with the Neurotron 1000.

## 1 Introduction

In radiosurgery, brain tumors (and other brain malformations) are destroyed by moving an intense beam of radiation [2, 6]. A necrotic dose is delivered to a tumor by cross-firing from multiple directions, to reduce the amount of energy deposited in healthy tissue. Although radiosurgery has been in use for several years, high ablative accuracy has only recently been made possible by progress in focused radiation sources and imaging techniques.

The radiosurgical treatment consists of several phases. First, a 3D map of the anatomical structures in the brain is constructed using CT and magnetic resonance (MR) techniques. Next a motion path for the radiation beam is computed to deliver a dose distribution that the surgeon finds acceptable (taking into account a variety of medical constraints). Finally, a jointed mechanism moves the radiation source according to this path.

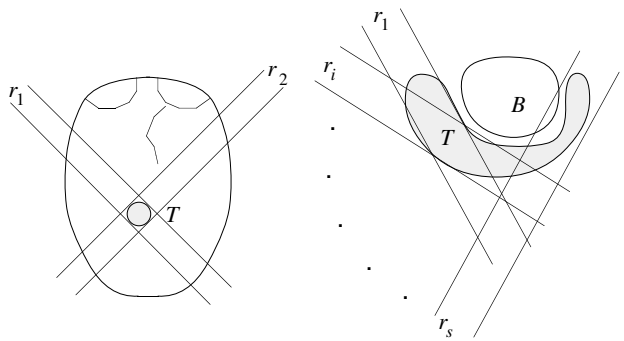


Figure 1: Cross-firing at a tumor

We consider the inverse dosimetry problem: Given a representation of anatomical structures and constraints on the dose to be absorbed by each structure, compute a sequence of beam configurations (positions and orientations) and dose weights for achieving the specified distribution. Fig. 1-a schematically shows an axial cross-section of the brain with a circular tumor $T$ and an optic nerve. If $T$ is irradiated from only one direction $r_1$, the healthy tissue along the beam absorbs approximately the same dose as the tumor. If, instead, we use two directions, $r_1$ and $r_2$, the dose deposited in the tumor is approximately twice the dose in healthy tissue. Using more beam directions can lead to further

improvements of the dose distribution. However, two additional issues must be considered:

• Healthy tissue should not always be treated uniformly. It usually contains critical and/or particularly sensitive regions (e.g., optic nerves, brainstem, blood vessels, spinal cord), which, to prevent severe post-operation side-effects, should receive at most very small doses. Such regions may considerably limit access to the tumor.

• The tumor shape must be taken into account in treatment planning. In many cases, cross-firing at a single center is not appropriate (fig. 1-b, where $B$ is a critical region). Furthermore, dose uniformity in the tumor is desirable. Excessive dose in some regions ("hot spots") may cause complications and should be avoided.

Earlier systems for radiosurgery (Gamma-Knife, LINAC-System [2, 6, 7, 8]) are restricted to a single isocenter treatment procedure, where all beams converge at a single point (the *isocenter*). This results in approximately spherical dose regions, i.e. a sphere around the isocenter will receive high dose. The example in Fig. 1-a illustrates this type of treatment. In the LINAC-System, beams can only be moved along circular arcs (*arc-treatment*). Given this restricted kinematics, non-spherical tumors must be approximated by several spheres, with each sphere treated separately. The number of spheres is limited, as the patient must be repositioned manually. (Typically no more than five isocenters are used). In order to avoid hot spots, the spheres thus produced should not overlap. For irregularly shaped tumors, it is generally difficult to avoid hot and/or cold spots.

In addition to kinematic limitations, earlier radiosurgical systems require that the patient's head be fixed rigidly in space. This is done with a *stereotactic frame*.

A new radiosurgical system based on a 6-dof manipulator allowing treatment of arbitrarily-shaped tumors has been implemented to overcome these limitations. We address the inverse dosimetry planning problem in the context of this system. Section 2 gives a system overview. Section 3 reviews previous work. Section 4 describes concepts of the geometric algorithms used for treatment planning. Section 5 describes the implemented planning system. Section 6 discusses a test series.

## 2 System Overview

The new radiosurgical system consists of the following components (fig. 2):

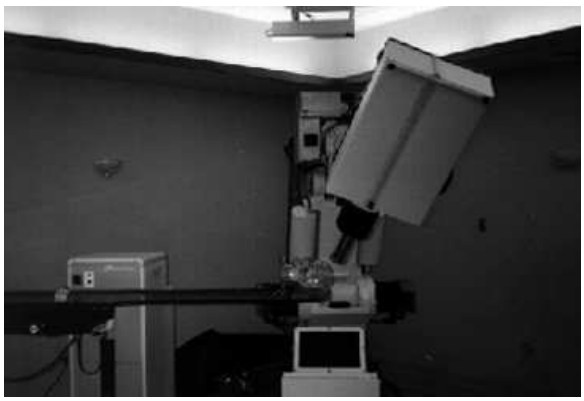

Figure 2: Radiation source and gantry, patient couch, water phantom, online x-ray vision system

• *Radiation source:* The radiation beam is generated by a 6 MV linear accelerator.

• *Mechanical gantry:* A GM-Fanuc 420 6-dof manipulator provides full kinematic flexibility for moving the radiation source. An ultrasonic system surveys the position of the robot.

• *Pre-operative Imaging:* CT and MR scanners are used to acquire pre-operative images of the brain. Fusion techniques merge the images into a 3D anatomical map.

• *Dynamic Vision:* An X-ray vision system made of two cameras acquires images of the patient's skull twice every second and computes the patient's position by correlating the images to precomputed radiographs. Small movements of the head are compensated for by a corresponding motion of the manipulator arm, while larger movements cause the radiation process to stop momentarily. Previous systems require the patient's head to be completely immobilized by using a painful stereotaxic frame fastened directly onto the skull with screws.

• *Treatment planning:* A planning system is used to compute beam paths for generating a desired dose distribution. The shape and relative location of anatomic structures varies greatly among patients. Even for the comparatively simple kinematics of earlier systems, manual treatment planning is time-consuming. In the case of a 6-dof arm, the planning process must be combined with kinematic computations and is obviously not suited for manual calculation.

• *Direct dosimetry:* A dosimetry program simulates the planned treatment and computes the dose distribution which will be generated by this treatment.

During treatment, the 6-dof arm moves in point-to-point mode through a series of configurations. At

each configuration, the beam is activated for a small time interval $\delta t$, while the arm is held still. The intensity of the beam is constant, hence $\delta t$ determines the dose delivered at each configuration. This duration can vary from one configuration to the next but is upper-bounded for patient protection.

To achieve an appropriate dose distribution within reasonable time the beam is activated at a series of 200 to 400 configurations. Beam activation and x-ray online imaging are synchronized, since no image can be taken during beam activation. Currently, the beam has a circular cross-section the radius of which remains constant throughout the same operation. However, this radius initially can be set between 5mm and 40mm by selecting an appropriate *collimator* for focusing the beam. In the future, variable multi-leaf or moving-slot collimators will allow the generation of beams with non-circular cross-sections.

## 3 Previous Work

The direct dosimetry problem is to compute the dose distribution in a tissue given a treatment plan. This computation relies on a fluence model for beams and tissue structures, derived from measurements in water phantoms (see e.g. [8, 9]). The inverse dosimetry problem is to find a treatment plan whose execution will achieve a desired dose distribution. Previous research has sought to find a mathematical solution for this problem by solving an integral equation: Given the desired dose distribution and the equation expressing the dose received at any one point as the integral over time of the fluence of the radiation beam, solve this integral for the fluence of the beam throughout the treatment. The approach is promising and progress has been reported over the last few years, notably in [1, 3, 5], but results remain restricted to simple distributions in the plane.

In [10] we proposed a geometric approach that consists of treating critical regions as obstacles that the radiation beam is not allowed to traverse. Given an approximately spherical tumor, the set of all beam directions passing through its center can be represented as the unit sphere $S^2$. The critical tissues map onto that sphere as regions of forbidden beam directions. From this representation, the planning system extracts a series of maximal vertical arcs along which to target the tumor. Such a plan fits the kinematic requirements of the LINAC-system (arc-treatment) but is restricted to the single-isocenter procedure described in section 1.

The new system offers the following advantages over earlier radiosurgical and radiotherapeutical systems (see e.g. [7, 8, 9]):

- The tissue does not have to be fixed in space. In earlier radiosurgical systems this was done with stereotaxic frames. Besides being very painful for the patient, this fixation was only possible for the lesions in the head, so the use of radiosurgical methods was limited.
- Based on geometric planning algorithms the radiation dose can be focused within the lesion with high accuracy so that healthy tissue can be protected, and side effects of radiation can be reduced dramatically. In particular, our algorithms allow for generating dose distributions with prescribed non-spherical isodosic surfaces and high homogeneity.

A prototype of the new system has been installed at Stanford Medical Center. The use of the system for clinical investigation was approved in February 1994.

## 4 Planning Approach

Throughout this section we assume that the radiation beam is generated by a circular collimator of given radius $r$.

**Principle:** A treatment plan consists of $n$ successive configurations of the manipulator. The radiation source is activated for a specified duration at each configuration.

Our planning method proceeds in two steps: First, we compute $n$ beam configurations using the anatomic map of the brain. Second, we compute the dose to be delivered at each beam configuration. The first step can be achieved in a variety of ways. In the next section we will propose one which provides good experimental results. Throughout this section we assume that the $n$ configurations have already been computed, and we focus on determining how they should be weighted.

Let $C_1, \ldots, C_n$ denote the cylinders at the $n$ selected configurations. We assign a dose value $w_i \geq 0$ to every $C_i$. The values $w_1, \ldots, w_n$ determine a dose distribution $D$. $D$ is defined as follows. If $p$ is a point and $C_1, \ldots, C_k$ are the cylinders containing $p$, then $D(p) = w_1 + \cdots + w_k$. (This definition gives a coarse model of photon beam characteristics. Refinements described below allow for a more accurate representation of these characteristics.)

We consider two disjoint regions $T$ (for tumor) and $H$ (for healthy tissue), with the following constraints:

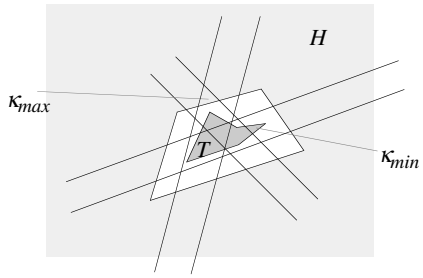


Figure 3: Regions $T, H$, minimal and maximal cell $\kappa_{min}$ resp. $\kappa_{max}$.

the dose delivered at each point in $T$ must be larger than some value $\alpha$, while the dose at each point of $H$ must be below $\beta$ ($\beta < \alpha$). The $n$ cylinders, $T$, and $H$ define an arrangement of *cells* in space. Each cell is defined as a maximal connected set not containing any piece of the boundaries of regions $T$ and $H$ or the cylinders. For each cell we compute a *label*. A cell $\kappa$ in cylinders $C_{i_1}, \ldots, C_{i_k}$ has label $l = \{i_1, \ldots, i_k\}$.

The calculation of $w_1, \ldots, w_n$ reduces to finding a point in the intersection of two $n$-dimensional polyhedral sets: If $\kappa$ is in $T$ and labeled by $\{i_1, \ldots, i_k\}$ then $\kappa$ determines the inequality:

$$\alpha \leq w_{i_1} + \cdots + w_{i_k}.$$

A cell $\kappa'$ labeled by $\{j_1, \ldots, j_{k'}\}$ in $H$ gives:

$$\beta \geq w_{j_1} + \cdots + w_{j_{k'}}.$$

The inequalities for all cells in $T$ determine an $n$-dimensional convex polyhedron $P_\alpha$. Similarly, the inequalities derived from the cells in $H$ determine a polyhedron $P_\beta$. If $P_\alpha$ and $P_\beta$ intersect, any point $(w_1, \ldots, w_n)$ in the intersection gives a dose distribution that satisfies the given constraints. Otherwise, the problem admits no solution.

More generally, we can specify several healthy critical or non-critical regions $H_1, \ldots, H_q$ marked by distinct maximal doses $\beta_1, \ldots, \beta_q$. We then obtain polyhedra $P_\alpha, P_{\beta_i}, \ldots, P_{\beta_q}$. Any point $(w_1, \ldots, w_n)$ in the intersection of these polyhedra determines a dose distribution that satisfies the input constraints.

The intersection of the polyhedra $P_\alpha, P_{\beta_1}, \ldots, P_{\beta_q}$ is an $n$-dimensional convex polyhedron. Extreme points of this set can be computed, allowing us to include optimality criteria (e.g., in addition to satisfying the input constraints defined by $\alpha, \beta_1, \ldots, \beta_q$, minimize the dose delivered to some region $H_i$).

**Reducing the number of inequalities:** We consider two inequalities deriving from two cells $\kappa$ and $\kappa'$ in $T$. Let $L = \{i_1, \ldots, i_k\}$ and $L' = \{j_1, \ldots, j_{k'}\}$ be the labels of $\kappa$ and $\kappa'$. If $L \subset L'$, then the inequality given by $\kappa$ implies the inequality given by $\kappa'$, since all $w_i$ are positive or null. A $T$-cell is called *minimal*, if its label is not a superset of any other $T$-label (figure 3). Similarly, a cell in $H_i$ is called *maximal*, if its label is not a subset of any other label in $H_i$. Thus, in the above polyhedral intersection test, we only need to consider inequalities stemming from minimal $T$-cells and maximal $H$-cells.

**Reduction in linear time:** The number of cells in an arrangement of $n$ cylinders is $\Theta(n^3)$. Assuming that $T$ and $H_1, \ldots, H_q$ have constant complexity, the total arrangement above also has $\Theta(n^3)$ cells. These cells, the associated inequalities, and the adjacency relationships between cells can be computed in nearly cubic time [4].

In our inequality set, we can delete all inequalities for non-minimal $T$-cells, as well as inequalities for non-maximal cells in $H_i$ (separately for each $i$). We conjecture that this gives better asymptotic bounds than the obvious bound of $O(n^3)$ for the number of remaining inequalities. Note that this conjecture only affects running time, but not correctness.

The above reduction can be done in time linear in the total number of cells: We traverse the cell arrangement in depth-first sequence. Between two adjacent cells $\kappa$ and $\kappa'$ in $T$ we traverse a cylinder wall. If the wall is traversed from the interior to the exterior of the cylinder, then $\kappa$ is non-minimal, so we can delete its label. On the other hand, if the cylinder wall is traversed from the exterior to the interior, then the label of the new cell $\kappa'$ is removed.[1] These relationships are reversed for pairs of adjacent cells in one of $H_i$.

**Approximating beam characteristics:** In reality the radiation beam does not behave exactly as a cylinder with constant fluence. The dose delivered by the beam decreases with distance to the beam's central axis. This decrease has been measured in clinical studies and can be represented by an exponential function [7]. In our method, we can obtain a more accurate model by representing a beam as a series of $p$ concentric cylinders. In the inequalities, the variables for the added cylinders occur with decreasing coefficients. The beam fluence also decreases with depth traveled in tissue [8]. To represent this effect, we can divide cylinders by planes orthogonal to their central

[1] Note that in general we do not delete all labels in this way. In fact, if this process terminates by deleting all labels, then the input problem has been found to be infeasible.

axis and adapt the coefficients in inequalities accordingly. A third effect observed in measurements is the beam widening with distance from the source. This effect can be taken into account by using cones instead of cylinders.

## 5 Implementation

A planning system based on the above methods was implemented in C on a Silicon Graphics Indigo workstation.

**Inputs:** The tumor and critical tissues are described as polyhedra. This is done as follows: the regions of interest are delineated by polygons in the MR images showing axial, sagital, or coronal cross-sections of the brain. These polygons are thickened by an amount corresponding to the distance between two consecutive cross-sections.

The planning system models the radiation beam as a cylinder of fixed radius with constant fluence. The radius $r$ of this cylinder and the number $n$ of beam configurations to consider are given as input. In practice, $n$ is limited by the total duration of the radiation procedure.

**Selection of beam configurations:** The first step of our planning approach consists of selecting beam configurations. We implemented and experimented with several techniques for this selection. The best results were obtained with the following technique.

Using an algorithm in [12], a grid of $n$ points is selected on the tumor surface. At each such point, a direction is randomly chosen on the upper half of a unit sphere in 3D, with uniform distribution.

A second method for selecting beam configurations was implemented in the planning system. In this method the surgeon specifies a line segment or polygonal sequence in the tumor. The system places evenly spaced isocenters along this segment or sequence. A series of beam directions is then generated for each isocenter. The reason for offering this method in the system is that it is a direct generalization of LINAC-procedures, for which there is a large amount of clinical experience. Note however, that as opposed to the LINAC-procedure, many spheres are overlaid with low dose.

With the second method, points in the tumor center absorb a much higher dose than points on the tumor surface. The first method avoids this drawback, but usually yields a slightly less sharp dose drop-off around the tumor.

**Computing dose weights:** Currently the arrangement of cylinders is computed using a fine regular grid of points in space, and determining the set of beams containing each grid point. A modified version of the revised simplex algorithm (RSM) is used to compute a point in the intersection of polyhedra in $n$ dimensions.

**Path generation:** The selected beam configurations must be organized into a sequence defining a path of the radiation source. For safety reasons, we currently do not consider optimization methods for finding this sequence. Instead, the computed beam configurations are inserted into a hard-coded sequence of via-points called *nodes*. The nodes provide a path template (fig. 4). For each node we precompute a local joint space. Thus, angle limits within which the arm can be moved without colliding or getting into the line of sight of a camera are associated with each node. The treatment beams are inserted in such a way that they are within the angular limits given with the nodes, thus giving a collision-free executable path.

The path shown in fig. 4 was executed and a photographic film in a water phantom (plexiglass reconstruction of a skull, placed at the end of the patient couch in fig. 2) was exposed to the generated radiation.

For this path equal dose was delivered at each node, with the beam axis aimed at the work space origin. The restrictions in the workspace (avoidance of camera occlusion) result in a penumbra along the horizontal direction in fig. 5 c and d (y-axis of workspace). A total of 6000 cGy was delivered at 300 nodes, resulting in a total execution time of 1 hour.

## 6 Test Series

A kernel of the implemented planning system has been extracted and prepared for clinical testing. This kernel is used interactively and comprises the following components:

- Beam selection; isocenters on line segments and isocenters on the tumor surface.
- Collision avoidance; beams computed by the beam selector are linked into a sequence of calibrated node configurations (fig. 4), avoiding workspace collisions, camera occlusion and arm posture changes.
- Beam weights; to allow for interactive computation the kernel planning system currently uses a simplified weighting scheme. Let $C_1, ..., C_k$ be all beams through critical regions. A value $\alpha$ is specified by the surgeon. The system then computes the minimum value $\beta$ s.t. dose $\alpha$ is achieved everywhere in the tumor when assigning weight $\beta$ to each of $C_1, \ldots, C_k$.

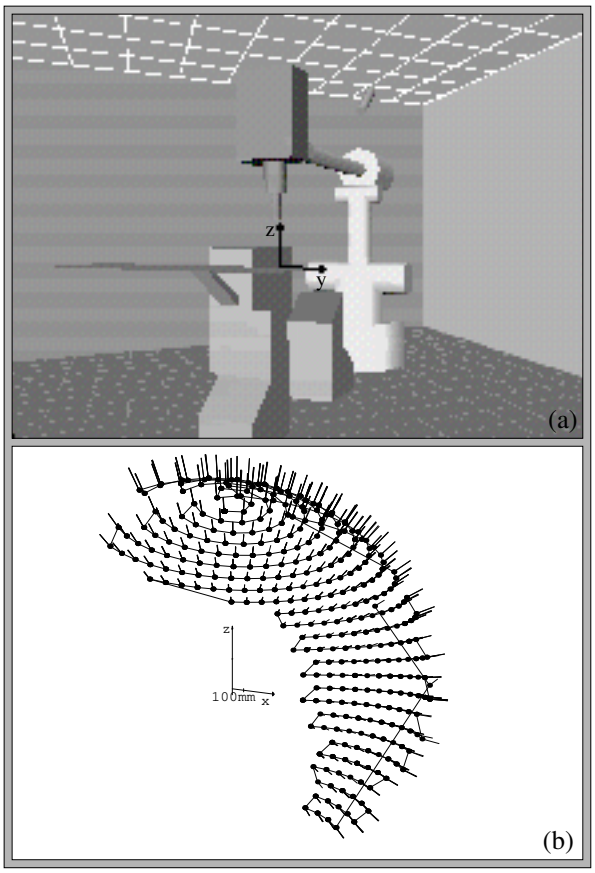


Figure 4: Template path connecting node configurations

• Direct dosimetry; three types of graphical visualization are available to the surgeon:

- Isodosic surfaces in 3D (an isodosic surface bounds the region that receives a dose greater than some specified value).

- Gray-level representation and isodosic curves in planar cross-sections.

- Dose-volume histograms (DVH) showing the volume (ordinate values) absorbing dose $\geq x$ as a function of $x$ (abscissa values). A separate DVH is computed for the tumor, critical tissue, and for tissue surrounding the tumor. Dose-volume histograms are particularly useful for evaluating dose homogeneity.

The capabilities of the new system with respect to generating improved dose distributions were analyzed in a test series using the planning system kernel. To allow for comparison we considered cases which previously had been treated with the LINAC-system. For spherical tumors, the methods in [10] give satisfactory results. Hence, we considered all cases which

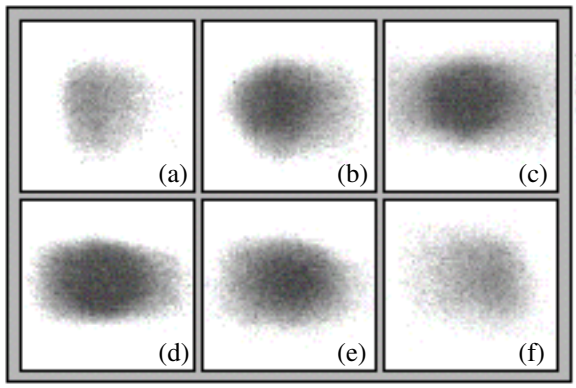


Figure 5: Phantom study for path in fig. 4 (spherical distribution, axial cross-sections)

had been treated at the Stanford Medical Center in the first quarter of 1993, in which more than one sphere was used to approximate the tumor. In total there were 12 such cases. Together with the case data and tomographic studies, the actual motions and dose weights were available. Based on this information we recomputed dose-volume histograms for tumor, critical organs as well as for the tissue surrounding the tumor, isodosic surfaces and dose distributions in cross-sections. Motions for the same cases, but now for the 6-dof system, were then generated and evaluated in the same way, and photographic film phantoms were established to verify direct dosimetry.

**Detailed case:** Fig. 6 shows the tumor of a 46 year-old woman in an axial cross-section at the level of the eyes. $T$ and $B$ denote the tumor and the brainstem respectively. Fig. 7 displays the polygons input to delineate these regions.

The recorded arc-treatment used two spheres to approximate the tumor. Fig. 8 shows the 50%-isodosic surface for this treatment (point set receiving 50% or more of the maximal dose), as well as the tumor polygons. The isodosic surface reveals the two spheres used to plan the treatment. A more detailed analysis shows that a hot spot is generated in the intersection of the two spheres (fig. 9).

Fig. 10 shows the 50%-isodosic surface obtained for the treatment generated by our planner (with $n = 300$). Fig. 11 displays the DVH in the tumor for three different plans. Black curve: recorded arc-treatment. Gray curve: treatment after the first step of our planner (all $n$ beams are evenly weighted). Light gray curve: treatment after minimizing the dose weight of the cylinders intersecting the brainstem. The DVH (fig. 11) shows that dose distribution in the tumor is more even with the second and third treatment. An

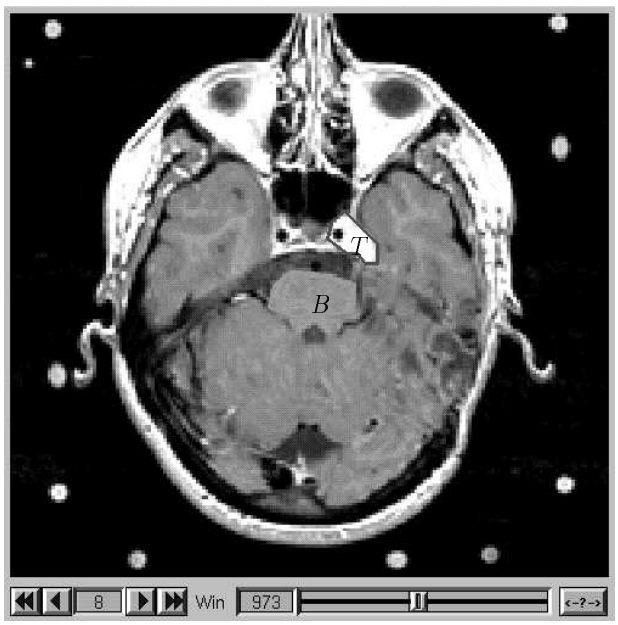


Figure 6: Anatomy for detailed case (+x-axis points to the left). Tumor region $T$, critical region $B$ (brainstem).

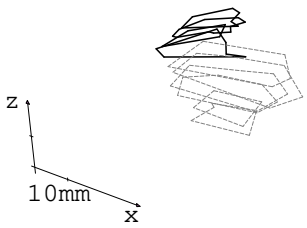


Figure 7: Polygons delineating brainstem (light gray) and tumor (black) for case in fig. 6

axial cross-section after weighting is shown in fig. 13. The dose in the brainstem is reduced to a large extent (lower right corner of fig. 13). Fig. 12 displays the DHV for the brainstem with the same three treatment plans. Much lower dose is deposited in the brainstem with the third treatment, while the dose in the surrounding tissue remains even.

## 7 Conclusion

Approval for clinical investigation using the prototype of the new system at Stanford Medical Center was given in February 1994. Systems will soon be installed at several major medical research institutions.

We divide treatment planning into two steps: (1)

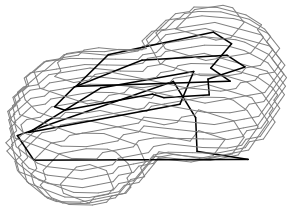

Figure 8: 50% Isodosic surface (arc-treatment with LINAC-System)

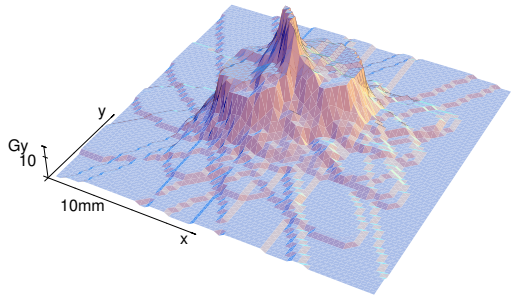


Figure 9: Dose distribution in axial slice for arc-treatment (1 Gy = 1 Joule/kg)

Selection of beam configurations. (2) Computation of dose weights for these configurations. For the second step, we proposed a general theoretical approach. The planning method relies on weighted arrangements in 3D. This is not limited to cylinders, and seems appropriate for treatment planning in conventional radiation therapy as well. This therapy is the dominant treatment procedure for cancer and radiates a larger region around a tumor site from three to five directions with comparatively low dose.

Currently, radiosurgical methods are limited to the brain, due to the necessity to rigidly fix tissue in space. The capabilty of the new system to track patient motion during treatment removes this limitation.

Preliminary studies suggest that the new system possesses the potential for revolutionary changes in cancer treatment. In particular, radiosurgical methods could now be used to treat cancer in all parts of the body, allowing for dose levels in tumors unachievable with conventional radiation therapy. This could allow for controlling tumors previously not treatable, and/or alleviate severe side-effects of conventional therapies in terminal cases.

Furthermore, radiosurgical treatment could be *fractionated*, i.e. delivered in 2-30 sessions instead of a single session. Fractionation is very effective in conventional radiation therapy, but so far has not been

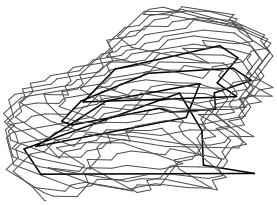

Figure 10: 50% Isodosic surface (planning system), black curves inside surface: tumor outline

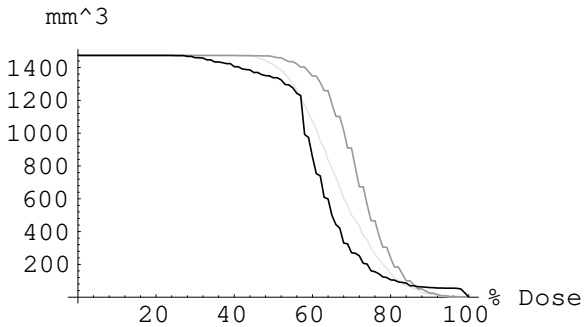


Figure 11: DVH's for tumor (black: arc treatment, gray: before weighting, light gray: after weighting

used in connection with radiosurgery, since the tissue would have to be fixed in space for each such session.

## References


[1] Barth, N. H. An Inverse Problem in Radiation Therapy. *Intern. J. Radiation Oncology Biol. Phys.*, 18:425–431, 1990.

[2] Betty, O. O., Munari, C., and Rosler, R. Stereotactic Radiosurgery with the Linear Accelerator: Treatment of Arteriovenous Malformations. *Neurosurgery*, 24(3):311–321, 1989.

[3] Brahme, A. Optimization of stationary and moving beam radiation therapy techniques. *Radiother. Oncol.*, 12:127-140, 1988.

[4] Chazelle, B., Edelsbrunner, H., Guibas, L., and Sharir. M. A singly-exponential stratification scheme for semi-algebraic varieties and its applications. In *Proc. 16th Int. Colloq. Automata Lang. Programm.*, Lecture Notes in Computer Science, Springer Verlag, 372:179–192, 1989.

[5] Cormack, A. A problem in rotation therapy with x-rays. *Int. J. Radiat. Oncol. Biol. Phys.*, 13:623-630, 1987.


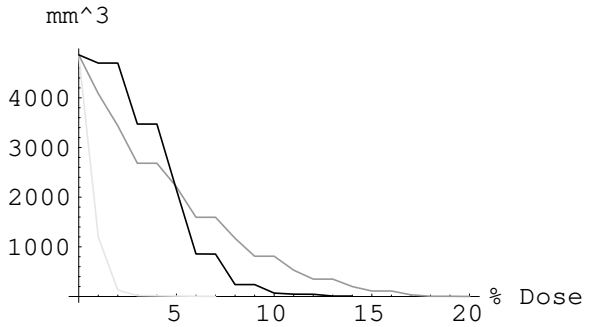


Figure 12: DVH's for brainstem

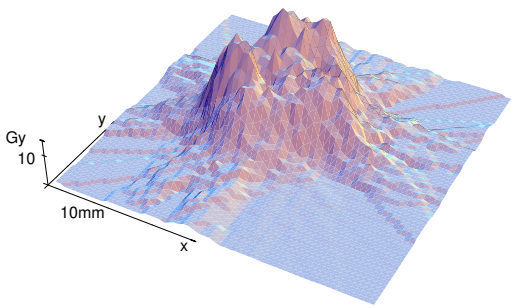


Figure 13: Axial cross-section after weighting


[6] Larsson, B. et al. The High Energy Proton Beam as a Neurosurgical Tool. *Nature*, 182:1222–1223, 1958.

[7] Lutz, W., Winston, K. R., and Maleki, N. A System for stereotactic radiosurgery with a linear accelerator. *Int. J. Radiation Oncology Biol. Phys.*, 14:373–381, 1988.

[8] Podgorsak, E. B., et al. Dynamic Stereotactic Radiosurgery *Intern. J. Radiation Oncology Biol. Phys.*, 14:115–126, 1988.

[9] Rice, R. K., et al. Measurements of Dose Distributions in Small Beams of 6 MeV X-Rays. *Phys. Med. Biol.*, 32:1087–1099, 1987.

[10] Schweikard, A., Adler, J. R., and Latombe, J. C., Motion Planning in Stereotaxic Radiosurgery. *Proc. IEEE Int. Conf. Robotics and Automation*, Atlanta, GA, May 1993, 1909–1916. (Extended version to appear in *IEEE Tr. Robotics and Automation.*)

[11] Troccaz, J. et al. Conformal External Radiotherapy of Prostatic Carcinoma: Requirements and Preliminary Results, Rep. No. 912I, TIMC-IMAG, Faculté de Médecine, Grenoble, 1993.

[12] Turk, G. Re-Tiling Polygonal Surfaces. *Computer Graphics*, 26(3):55–64, 1992.